Physica B 424 (2013) 42–46

Contents lists available at SciVerse ScienceDirect

Physica B

journal homepage: www.elsevier.com/locate/physb

Bound magnetic polaron driven low-temperature ferromagnetism in $Cu_{1-x}Mn_xO$ compounds

J.Z. Cai, L. Li, S. Wang, W.Q. Zou, X.S. Wu *, F.M. Zhang *

National Laboratory of Solid State Microstructures, Department of Physics, Nanjing 210093, China

ARTICLE INFO

Article history:
Received 22 February 2013
Received in revised form
7 May 2013
Accepted 10 May 2013
Available online 24 May 2013

Keywords:
Mn-doped CuO
Ferromagnetism
Carrier concentration
Bound magnetic polaron (BMP)

ABSTRACT

Partial Mn atoms have been confirmed to enter the CuO lattice and form the $Cu_{1-x}Mn_xO$ compounds in the case of doping with $0 \le x \le 0.2$ by the sol–gel method. With increasing Mn content, magnetism is observed. The magnetic critical transition temperature increases with enhanced magnetism, which obeys the bound magnetic polaron theory. The electronic transportation shows an insulating behavior as the band-gap decreases. Our results may indicate that CuO may be used as a candidate of magnetic semiconductor.

1. Introduction

The origin of ferromagnetism in semiconductors is one of the most important issues for physics of magnetism [1–3] and device applications at present [4,5]. Since Dietl et al. [6] found that the magnetic properties for semiconductors could be affected by carriers and doping, great effort has been devoted. Particularly, ferromagnetism of transition metal oxides (TMOs) attracted more attention for the 3d electrons induced strong coupling among spin, charge, orbital and vibration degrees of freedom, such as Fe-doped

balance in structural and magnetic properties [15,16]. Ferromagnetism (FM) has been obtained in transition-metal-doped CuO and many theoretical works have been developed to explore the origin of the FM in doped CuO system. An unconventional double-exchange model, which is consistent with experimental results of Yang et al. [17] and Zhang et al. [18], was proposed by Filippetti et al. [19] to explain the FM in Mn-doped CuO. However, high carrier density is required in the double-exchange model while several studies reported FM in samples with low carrier density [20,21]. Furthermore, some groups reported room temperature FM in un-doped CuO nanostructures [22–25]. The oxygen vacancies, uncompensated surface spins or surface effect at the grain boundary may result in FM in CuO although the FM is weak compared to that of Mn doped CuO. Here, we study the relationship between FM and Mn doping concentration of $Cu_{1-x}Mn_xO$ ($x=0.06$, 0.1, and 0.2) samples since phases Mn_2O_3 and Mn_3O_4 might appear along with the higher doping concentration, and we support the BMP [26] model for the original of FM in the low carrier density Mn doped CuO system.

Polycrystals of $Cu_{1-x}Mn_xO$ ($x=0$, 0.06, 0.1, and 0.2) are synthesized by the sol–gel method [27] The starting solutions for the deposition of Mn-doped CuO are prepared by dissolving copper nitrate [$Cu(NO_3)_2 \cdot 6H_2O$] and manganese nitrate [$Mn(NO_3)_2$] in de-ionized water. Thereafter, citric acid was added to the solution. The solution was stirred for 3 h at 75 °C. Afterward, ethylene glycol was added to the resulting solution which is to be stirred until it transforms into gel. The gel is dried in air for 20 h and then ground for 30 min before annealing. The as-prepared powder is annealed at 500 °C in air for 1 h and then formed into pellets by sintering at 400 °C in air for 6 h.

The structure of the $Cu_{1-x}Mn_xO$ ($x=0$, 0.06, 0.1, and 0.2) samples is characterized at room-temperature by X-ray diffraction (XRD) performed on a Rigaku Dmax-rb in the step scanning mode with a step size of 0.02° in 2θ. The magnetization curves are measured in a commercial superconducting quantum interference

* Corresponding authors. Tel.:+86 258359 4402.
E-mail addresses: xswu@nju.edu.cn (X.S. Wu), fmzhang@nju.edu.cn (F.M. Zhang).

0921-4526
http://dx.doi.org/10.1016/j.physb.2013.05.007

device (SQUID, MPMS-XL) magnetometer. And the electric transport properties are measured by the four-point probe method.

3. Results and discussions

Fig. 1 shows the XRD patterns of the $Cu_{1-x}Mn_xO$ ($x=0$, 0.06, 0.1, and 0.2) samples. Rietveld refinements using the laboratory X-ray diffraction (XRD) data [28,29] and synchrotron radiation data obtained in Shanghai Synchrotron Radiation Facility (SSRF) on beam line BL14B1 with the computer code of the General Structure Analysis System (GSAS) are performed. A slight amount of $CuMn_2O_4$ is detected and added to the refinements. The refinement procedure is performed as reported previously [30,31]. The space groups $C12/c1$ for $Cu_{1-x}Mn_xO$ and $I4/amd$ for $CuMn_2O_4$ fit the XRD pattern. CuO (data_16025-ICSD) and $CuMn_2O_4$ (data_9812-ICSD) are used as the starting models. We set that Mn atoms substitute Cu atoms in CuO lattice. The scale factor is refined initially, and later the phase fractions; after that we use function type 5 to refine background. The lattice parameters, peak shape, preferential orientation, the atom position and Uiso of the two phases are refined separately, step by step. The collected XRD spectra, together with the refined patterns of all the samples are shown in Fig. 1(b). The refined unit cell, atomic parameters, including the lattice constants, the bond lengths, the bond angles, the atomic position and content of the phases are summarized and listed in Table 1. The occupancy of Mn at Cu in CuO in our samples is fitted to be 0, 0.040, 0.061, and 0.128 for $Cu_{1-x}Mn_xO$ with $x=0$, 0.06, 0.1, and 0.2, respectively, which is consist with the original reactants.

The temperature-dependent resistivity for $Cu_{1-x}Mn_xO$ ($x=0.06$, 0.1, and 0.2) is shown in Fig. 2(a) in the semi-log scale. Resistivity decreases with the doping concentration, suggesting the enhancement of carrier density. The activation energy can be calculated with the thermal-activated model $\rho \propto \rho_0 \exp(-\frac{E_a}{K_B T})$ and the values of E_a are 0.228, 0.151, and 0.153 eV for $x=0.06$, 0.1, and 0.2, respectively. All the samples show the insulating behavior. Fig. 2 (b) shows the temperature dependence of resistivity for the sample of $Cu_{0.8}Mn_{0.2}O$. The large resistivity indicates low carrier concentration below T_c in the samples.

The hysteresis loops for $Cu_{1-x}Mn_xO$ ($x=0$, 0.06, 0.1, and 0.2) samples are shown in Fig. 3. The values of M_s, M_r and H_c, T_c for $Cu_{1-x}Mn_xO$ ($x=0.06$, 0.1, and 0.2) samples are listed in Table 2. According to the results reported by Yang et al. [19], the $CuMn_2O_4$ phase does not contribute to the hysteresis. Only weak FM is observed in the Mn-free CuO sample. The magnetic moment is about 4×10^{-3} emu/g and could be ascribed to the uncompensated surface spins or surface effect at the grain boundary. However, much stronger FM is observed in Mn-doped CuO at low temperature. This distinguishes the origin of FM for Mn-doped CuO from the un-doped CuO in our experiment, and indicates that the FM of Mn-doped CuO must be originated by Mn ions substituting Cu ions into CuO matrix. The magnetic moment is 5.67 emu/g for $Cu_{0.94}Mn_{0.06}O$, 11.44 emu/g for $Cu_{0.9}Mn_{0.1}O$ and 21.95 emu/g for $Cu_{0.8}Mn_{0.2}O$. The magnetic moment for each Mn atom increases with the dope concentration from $1.94\mu_B$/atom to $2.66\mu_B$/atom and $2.77\mu_B$/atom. All these magnetic moments are far away from the theoretic value of Mn^{2+}. As the hysteresis loop does not saturate even at 10 kOe, a large number of paramagnetic moments should coexist with the ferromagnetic moment. The coercive fields remain around 200 Oe for S1–S3.

Fig. 4 shows the magnetic moment versus temperature curves for $Cu_{1-x}Mn_xO$ ($x=0.06$, 0.1, and 0.2) samples under 100 Oe magnetic field in the temperature range of 4–150 K. The Mn doped CuO

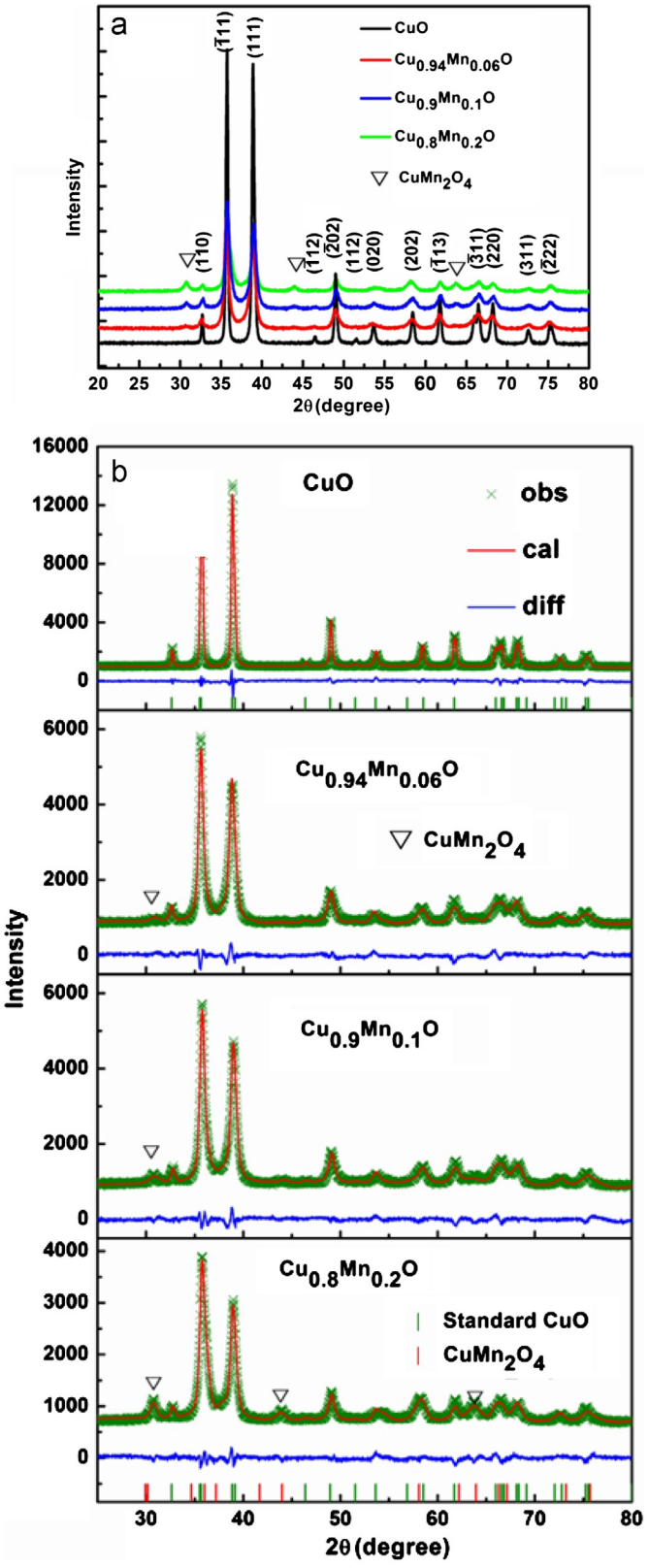

Fig. 1. (a) XRD spectrum of polycrystals of $Cu_{1-x}Mn_xO$ ($x=0$, 0.06, 0.1, and 0.2) compounds. (b) Observed and calculated XRD profiles of Rietveld refinements for $Cu_{1-x}Mn_xO$ ($x=0$, 0.06, 0.1, and 0.2) separately, along with the plots of the difference between the observed and calculated profiles. The vertical short lines (red and green) represent the position of Bragg reflection of CuO and $CuMn_2O_4$ respectively. (For interpretation of the references to color in this figure legend, the reader is referred to the web version of this article).

samples show clearly FM transition and the Curie temperature (T_c) increases with increasing Mn content x; otherwise the Mn-free CuO shows only a slight magnetic moment. The inset of Fig. 4 shows temperature dependence of inverse susceptibility. We extrapolate $1/M$ versus T to define the Curie temperature (T_c) of $Cu_{1-x}Mn_xO$ ($x=0.06$, 0.1, and 0.2) according to the Curie–Weiss law. The positive Weiss constant suggests that this transition is between paramagnetic and FM phases. The Curie–Weiss temperature of $Cu_{1-x}Mn_xO$ ($x=0.06$, 0.1, and 0.2) is 76.6 K, 80.1 K, and 82.3 K, respectively.

Considering the low carrier density and unsaturated hysteresis loop of $Cu_{1-x}Mn_xO$ ($x=0.06$, 0.1, and 0.2) samples, the FM behavior may be explained by the BMP model [26], which can work in high resistivity samples because their mediate carriers are localized. The BMPs in Mn-doped CuO system, sketched in Fig. 5, consist of a

Table 1
Refined atomic parameters for $Cu_{1-x}Mn_xO$ ($x=0$, 0.06, 0.1, and 0.2) are summarized and listed. The composition of the impurity $CuMn_2O_4$ (CM124) phase is also given in the table.

X	0	0.06	0.1	0.2
a (Å)	4.6764(1)	4.6690(3)	4.6697(3)	4.6741(4)
b (Å)	3.4201(0)	3.4309(2)	3.4206(2)	3.4234(2)
c (Å)	5.1245(1)	5.1233(4)	5.1221(3)	5.1254(5)
α (deg)	90	90	90	90
β (deg)	99.383(2)	99.374(6)	99.328(6)	99.311(8)
γ (deg)	90	90	90	90
V (Å^3)	80.867(3)	80.977(10)	80.733(10)	80.933(13)
Cu^{2+}/Mn^{2+}				
x	0.25	0.25	0.25	0.25
y	0.25	0.25	0.25	0.25
z	0	0	0	0
Uiso(Cu/Mn)O^{2-}	0.017	0.018/0.025	0.021/0.017	0.023/0.014
x	0	0	0	0
y	0.4206(7)	0.4479(11)	0.4595(11)	0.4623(14)
z	0.25	0.25	0.25	0.25
Uiso	0.028	0.011	0.024	0.016
Bond length				
Cu(Mn)–O	1.9589(10)	1.9878(13)	2.0050(14)	2.0053(18)
Cu(Mn)–O	1.9464(5)	1.8947(21)	1.8719(20)	1.8688(26)
Bond angle				
O–Cu(Mn)–O	84.236(16)	83.509(24)	83.343(18)	83.264(24)
O–Cu(Mn)–O	95.764(16)	96.491(24)	96.657(18)	96.736(24)
Cu(Mn)–O–Cu(Mn)	145.33(9)	140.040(21)	138.000(11)	137.480(26)
Cu(Mn)–O–Cu(Mn)	104.148(18)	105.112(29)	105.333(17)	105.356(29)
Fraction of CM124	0	0.011	0.0257	0.065
Mn content in CM	0	0.042	0.061	0.128
Rp (%)	4.04	4.08	3.93	3.95
Rwp (%)	3.16	3.21	3.14	3.11

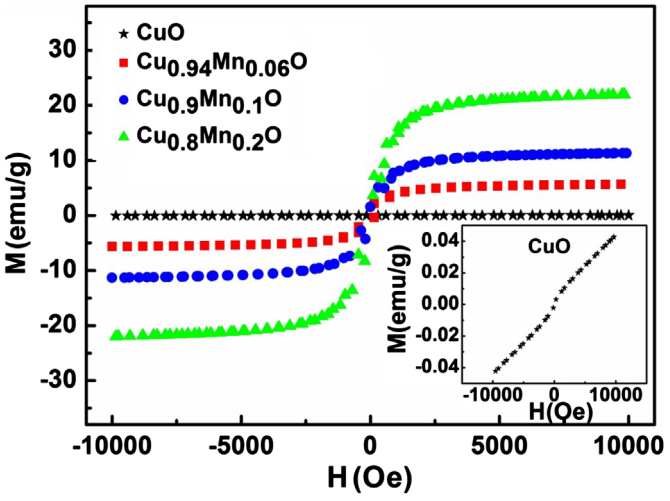

Fig. 3. Magnetic hysteresis loops for $Cu_{1-x}Mn_xO$ ($x=0$, 0.06, 0.1, and 0.2) samples at 4 K.

Table 2
The values of M_s, M_r and H_c, T_c for $Cu_{1-x}Mn_xO$ ($x=0.06$, 0.1, and 0.2) samples are listed.

x	0.06	0.1	0.2
M_s (emu/g)	5.67	11.94	21.95
M_r (emu/g)	1.45	2.62	3.95
H_c (Oe)	180	185	170
T_c (K)	76.6	80.1	82.3

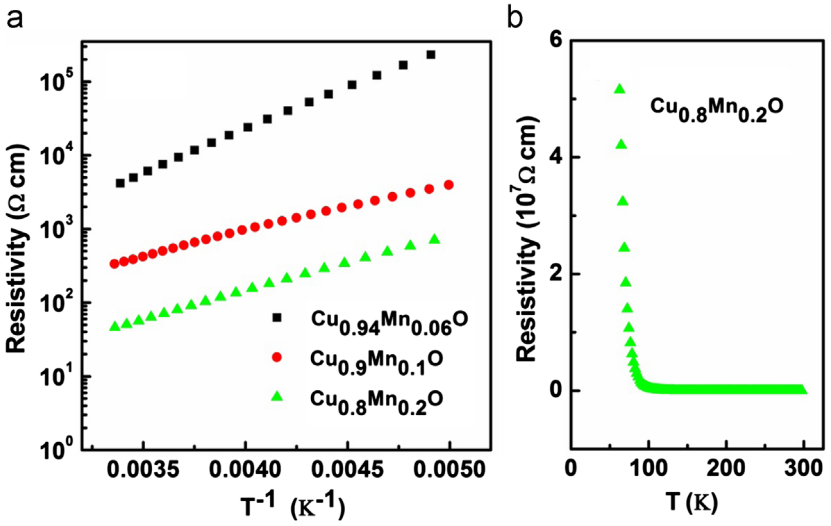

Fig. 2. (a) Temperature dependence of electrical resistivity in semi-log scale of $Cu_{1-x}Mn_xO$ ($x=0.06$, 0.1, and 0.2) samples. (b) Resistivity versus T curve for $Cu_{0.8}Mn_{0.2}O$ sample.

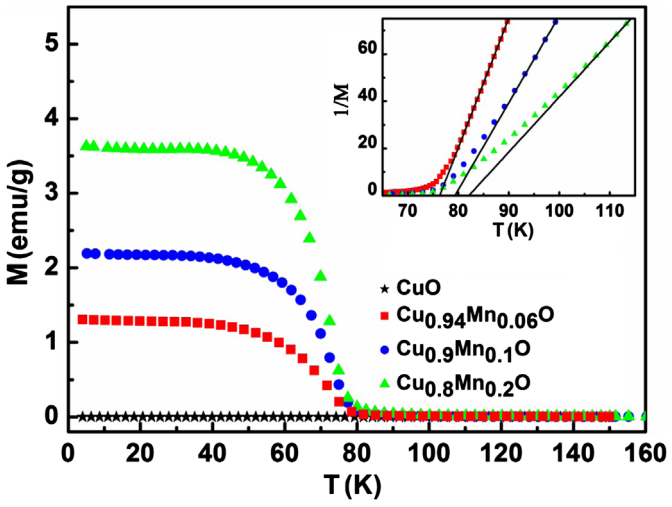

Fig. 4. Temperature dependence of magnetization for $Cu_{1-x}Mn_xO$ ($x=0$, 0.06, 0.1, and 0.2) samples with 100 Oe applied. The inset is $1/M$ versus T curves.

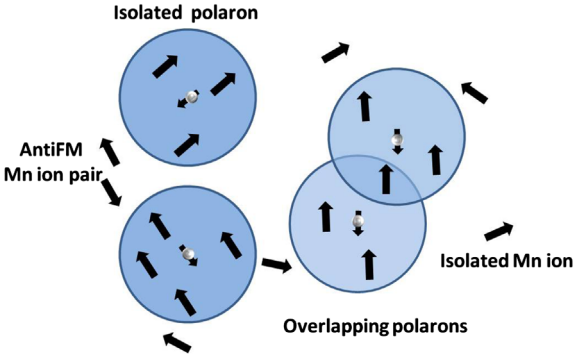

Fig. 5. Bound magnetic polaron model in $Cu_{1-x}Mn_xO$ system is sketched. The polarons are shown in blue circle. The white balls with little arrows represent hole spins and the big arrows represent Mn^{2+} spins. (For interpretation of the references to color in this figure legend, the reader is referred to the web version of this article).

localized hole and the surrounded Mn^{2+} ions. The interexchange interaction between Mn^{2+} ions as well as Mn^{2+} ions and Cu^{2+} ions induces antiferromagnetism which is weak compared to the ferromagnetism. According to Durst's model [32], the interaction between two polarons could be described as

$$H_m = K[(s_1S_1)+(s_2S_2)]+K'(s_1+s_2)S_3+Js_1s_2 \quad (1)$$

where K is the exchange constant of the hole–ion interaction within the polaron, K' is the exchange constant of the interaction between the hole and ion in the overlapping region, and J is the direct antiferromagnetic hole–hole exchange ($J \ll K$ in our samples). Parameters s_1 and s_2 are the hole spins, S_1 and S_2 are the sum of the Mn ion spins in each polaron, and S_3 is the sum of Mn spins in the overlapping region. The first item in Eq. (1) represents the hole–ion interaction, which antialigns the spins of Mn ions around a hole in relation to the hole spin in a polaron. As a result, a single polaron with a large collective spin forms. In a polaron-pair system, when the two polarons have a overlapping region, the polarons interact via the indirect hole–ion–hole interaction, described by the second term in Eq. (1), which makes the both polarons antialign with the nearest Mn ions. Thus, the long-range FM coupling originates from the overlapping and interactions between two neighboring BMPs at low temperature. In an ideal model, assuming that the collective moment of the sample is along the z-axis, we suggest that

$$\mu_{Jz} = \sum_{j=1}^{M}\left(\sum_{i=1}^{N_j}\mu_{Jz_i}-\mu'_{Jz_j}\right) \quad (2)$$

where μ_{Jz} is the collective moment of the sample, μ_{Jz_i} is the Mn ion moment along the z-axis, μ'_{Jz_j} is the moment of hole, N_j is the number of Mn ions in one polaron, and M is the number of the aligned polarons. Increasing hole concentration would increase the amount of BMPs; meanwhile, the enhancement of Mn^{2+} ions improves the amount of Mn^{2+} ions contained in the BMP system. As a consequence, these BMPs induce stronger FM interaction through both magnetic moments and Curie–Weiss temperatures. This is quite consistent with our experiment results that magnetic moments increase with the enhancement of Mn doping.

4. Conclusion

Low temperature ferromagnetism (FM) has been observed in $Cu_{1-x}Mn_xO$ ($x=0.06$, 0.1, and 0.2) samples with $T_c > 75$ K. Compared to the Mn-free CuO, the FM is confirmed to be originated from Mn doping. Ferromagnetic transition temperature and the saturation moment increase with increasing Mn doping. The ferromagnetism is in excellent fit with the bound magnetic polaron mechanism. The insulating behavior in Mn-doped CuO supports the magnetic model.

Acknowledgments

This work is supported by Nature Science Foundation of China (Nos. 11274153, and 11204124), and the National Key Projects for Basic Researches of China (2010CB923404). The authors thank beam line BL14B1 (Shanghai Synchrotron Radiation Facility) for providing beam time.

References

[1] F.M. Zhang, X.C. Liu, J. Gao, X.S. Wu, Y.W. Du, H. Zhu, J.Q. Xiao, P. Chen, Appl. Phys. Lett. 85 (5) (2004) 786.
[2] X.C. Liu, Z.H. Lu, Z.L. Lu, L.Y. Lv, X.S. Wu, F.M. Zhang, Y.W. Du, J. Appl. Phys. 100 (07) (2006) 3903.
[3] Q.Y. Xie, M.Q. Gu, L. Huang, F.M. Zhang, X.S. Wu, AIP Adv. (2012)012185.
[4] J.P. Xu, Y.B. Lin, Z.H. Lu, X.C. Liu, Z.L. Lu, J.F. Wang, W.Q. Zou, L.Y. Lv, F.M. Zhang, Y.W. Du, Solid State Commun. 140 (11) (2006) 514.
[5] X.C. Liu, Y.B. Lin, J.F. Wang, Z.H. Lu, Z.L. Lu, J.P. Xu, L.Y. Lv, F.M. Zhang, Y.W. Du, J. Appl. Phys. 102 (03) (2007) 3902.
[6] T. Dietl, H. Ohno, F. Matsukura, J. Cibert, D. Ferrand, Science 287 (5455) (2000) 1019.
[7] J.M.D. Coey, A.P. Douvalis, et al., Appl. Phys. Lett. 84 (8) (2004) 1332.
[8] Y.X. Li, M. Xu, L.Q. Pan, Y.P. Zhang, Z.G. Guo, J. Appl. Phys. 107 (2010) 113908.
[9] R. Asmatulu, H. Haynes, M. Shinde, Y.H. Lin, Y.Y. Chen, J.C. Ho, J. Nanomater. 2010 (2010) 71582.
[10] Qingyu Xu, Zheng Wen, Liguo Xu, Jinlong Gao, Di Wu, Kai Shen, et al., Phys. B: Condens. Matter 46 (2011) 19.
[11] R.K. Singhal, P. Sudhish Kumar, Y.T. Kumari, E. Xing, Saitovitch, Appl. Phys. Lett. 98 (2011) 092510.
[12] R.K. Singhal, P. Kumari, A. Samariya, S.C. Sudhish Kumar, Y.T. Xing, Saitovitch, Appl. Phys. Lett. 97 (2010) 172503.
[13] T. Kimura, Y. Sekio, H. Nakamura, T. Siegrist, A. Ramirez, Nat. Mater. 7 (2008) 291.
[14] S. Asbrink, L. Norrby, Acta Crystallogr. Sect. B 26 (1970) 8.
[15] J. Zaanen, G.A. Sawatzky, J.W. Allen, Phys. Rev. Lett. 55 (1985) 418.
[16] M. Ain, W. Reichardt, B. Hennion, G. Pepy, B.M. Wanklyn, Physica C 162 (1989) 1279.
[17] S.G. Yang, T. Li, B.X. Gu, Y.W. Du, Appl. Phys. Lett. 83 (2003) 3746.
[18] Y.P. Zhang, L.Q. Pan, Y.S. Gu, F. Zhao, H.M. Qiu, J.H. Yin, H. Zhu, John Q. Xiao, J. Appl. Phys. 105 (2009) 086103.

[19] A. Filippetti, V. Fiorentini, Phys. Rev. B 74 (2006) 220401.
[20] K.H. Gao, Z.Q. Li, T. Du, En Yong Jiang, Phys. Rev. B 75 (17) (2007) 4444.
[21] S. Philip Raja, D. Paul Joseph, C. Venkateswaran, Mater. Chem. Phys. 113 (2009) 67.
[22] D.Q. Gao, G.J. Yang, J.Y. Li, J. Zhang, J.L. Zhang, D.S. Xue, J. Phys. Chem. C 114 (18) (2010) 347.
[23] J.G. Zhao, S.J. Liu, S.H. Yang, S.G. Yang, Appl. Surf. Sci. 257 (22) (2011) 9678.
[24] S. Das, S. Majumdar, S. Giri, Appl. Surf. Sci. 257 (24) (2011) 10775.
[25] J.W. Chen, G. Narsinga Rao, IEEE Trans. Magn. 47 (10) (2011) 3772.
[26] A. Kaminski, S. Das Sarma, Phys. Rev. Lett. 88 (24) (2002) 7202.
[27] Y.C. Hu, Z.Z. Jiang, K.G. Gao, G.F. Cheng, J.J. Ge, X.M. Lv, X.S. Wu, Chem. Phys. Lett. 534 (2012) 62.
[28] H. Sha, X.S. Wu, Y.M. Xu, A. Hu, S.S. Jiang, J. Superconductivity: Incorporating Novel Magn. 17 (2) (2004) 247.
[29] X.S. Wu, J. Gao, Physica C: Superconductivity 313 (1999) 79.
[30] X.S. Wu, S.S. Jiang, J. Lin, J.S. Liu, X. Jin, Physica C: Superconductivity 309 (1998) 25.
[31] X.S. Wu, J. Gao, Physica C: Superconductivity 315 (1999) 215.
[32] Adam C. Durst, R.N. Bhatt, P.A. Wolff, Phys. Rev. B 65 (23) (2002) 5205.